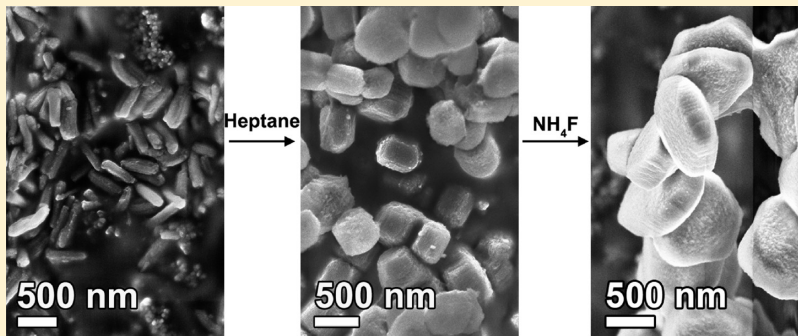


## Tuning the Shape of Mesoporous Silica Particles by Alterations in Parameter Space: From Rods to Platelets

Emma M. Björk, Fredrik Söderlind, and Magnus Odén\*

Nanostructured Materials, Department of Physics, Chemistry and Biology, Linköping University, Linköping SE-58183, Sweden

Supporting Information



**ABSTRACT:** The knowledge of how to control the pore size and morphology of separated mesoporous silica particles is crucial for optimizing their performance in applications, such as molecular sieves and drug delivery systems. In this work, we have systematically studied the effects of various synthesis parameters to gain a deeper understanding of how particle morphologies can be altered. It was found that the morphology for isolated particles of SBA-15 type, with unusually short and wide pores, could be altered from rods to platelets by variations in the  $\text{NH}_4\text{F}$  concentration. The pore length is nearly constant ( $\sim 300 \text{ nm}$ ) for the different morphologies, but the particle width is increasing from  $200 \text{ nm}$  to  $>3 \mu\text{m}$  when decreasing the amount of  $\text{NH}_4\text{F}$ , and the pore size can be tuned between  $10$  and  $13 \text{ nm}$ . Furthermore, other synthesis parameters such as heptane concentration, pH, silica precursor, and additions of ions have also been studied. The trend regarding particle width is independent of heptane concentration, at the same time as heptane increases the particle length up to a plateau value of  $\sim 500 \text{ nm}$ . In all, parameters controlling particle width, length, and pore size have been separated in order to evaluate their function in the particle formation. Additionally, it was found that the formation time of the particles is strongly affected by the fluoride ion concentration, and a mechanism for particle formation for this system, where micelles transform from a foam, to multilamellar vesicles, and finally to cylindrical micelles, is suggested.

### INTRODUCTION

Mesoporous materials have, since the discovery in the early 1990s, been given much attention due to their many possible applications such as catalysis, drug delivery systems, gas sensors, molds for nanoparticles, etc.<sup>1–6</sup> The SBA-15 type of materials<sup>7</sup> is one of the most commonly studied among the mesoporous materials due to its straight cylindrical pores and tunable pore size. Lately, it has been shown that the shape of the particles can have large effects on their performance when used in an application, and especially isolated particles have shown to be favorable. For example, short particles with easy access to the pores are favorable in catalytic applications,<sup>8,9</sup> enzyme immobilization,<sup>10–12</sup> and drug delivery systems.<sup>13</sup> These types of particles are most often rod shaped, but also platelets are of interest in various applications, due to the high accessibility of the pores and the large specific surface area.<sup>14</sup>

In order to control the particle length and shape, several synthesis parameters have been studied over the years, and morphologies such as fibers, spheres, films, platelets, and cuboids have been formed. Decreasing the stirring time yields

isolated particles, rods,<sup>15,16</sup> but continued tailoring of the particle morphology and pore size is crucial for their performance in applications. Alterations of the synthesis conditions such as additions of salts have shown to be favorable for increasing the order in particles,<sup>17</sup> rods synthesized under certain conditions elongate upon a decrease of the HCl concentration,<sup>18,19</sup> and rods can be transformed from rods to platelets when the amount of sodium silicate, used as the silica precursor, is increased.<sup>20</sup> An alternative route to synthesize platelets is to use P104 as surfactant instead of P123<sup>21–23</sup> or by adding Zr ions.<sup>24,25</sup> It is also possible to tune the pore size of the isolated particles by e.g. swelling agents such as 1,3,5-triisopropylbenzene<sup>26</sup> or to remove the microporosity by salt additions at certain steps in the synthesis.<sup>27</sup> Since there are so many variables to alter, it is obvious that a detailed knowledge of the formation of the mesoporous

**Received:** August 19, 2013

**Revised:** October 8, 2013

**Published:** October 9, 2013

material and to map and understand how each parameter specifically affect the final material.

The low reaction temperature system used in this study, with additives such as heptane and  $\text{NH}_4\text{F}$ ,<sup>28–30</sup> is not as well explored compared to the ordinary SBA-15 system. Even though morphologies such as sheets,<sup>28,29</sup> fibers,<sup>29</sup> and separated rods<sup>30</sup> have been reported, the formation of the material has not been studied in detail. This synthesis route is of interest, since it yields particles of SBA-15 type, but with wider and shorter pores than usual. Previous studies of similar systems with alternative alkanes have shown that the particle length is affected by the length of the alkane.<sup>31</sup> It has also been shown that the TEOS concentration transform the material from a fiber morphology to monoliths,<sup>31</sup> and cuboids with pores running through the short axis of the particle can be formed if the alkane is added at a different time.<sup>32</sup> Furthermore, it is possible to synthesize large pore materials with pores larger than 20 nm if Pluronic F127 is combined with FC-4 surfactants in a similar low-temperature synthesis.<sup>33,34</sup>

Here we further explore the parameter space for the low reaction temperature synthesis, which includes both heptane and  $\text{NH}_4\text{F}$  and yields isolated mesoporous silica particles with pores larger than 10 nm. Previously unstudied parameters such as ion concentrations, heptane amount, salt additions, and silica precursor have been explored in order to deepen the understanding of what decides the particle morphology and growth behavior. Also, a more generalized study of the effect of pH was performed in order to prove previously presented results, indicating the possibility to tune rod length by alteration in the HCl concentration.<sup>30</sup> The present study has yielded separated particles with rod and the unusual platelet morphology, with large pores easily accessible from the (001) surface of the particles, for which the aspect ratios can be tuned. Further, the formation of these particles has been studied and is shown to differ compared to the formation of the commonly used SBA-15 synthesis route since it includes steps of foams and multilamellar vesicles (MLVs).

## ■ EXPERIMENTAL METHODS

**Synthesis.** Hydrochloric acid (purity  $\geq 37\%$ , puriss. p.a., Fluka, ACS Reagent, fuming), triblock copolymer  $\text{EO}_{20}\text{PO}_{70}\text{EO}_{20}$  (P123) (Aldrich), tetramethyl orthosilicate (TMOS), tetraethyl orthosilicate (TEOS) (reagent grade, 98%, Aldrich), heptane (99%, ReagentPlus, Sigma-Aldrich), sodium chloride, ammonium fluoride (purity  $\geq 98.0\%$ , puriss. p.a., ACS reagent, Fluka), and ammonium chloride (purity  $\geq 98.0\%$ , Scharlau) were used as received.

In a typical synthesis, 2.4 g of P123 and a given amount of  $\text{NH}_4\text{F}$  were dissolved in 80 mL of 1.94 M HCl solution. The mixture was kept at 20 °C and stirred until the polymer was dissolved. Various volumes of heptane were premixed with 5.5 mL of TEOS and added to the micellar solution. The synthesis was stirred for 4 min and then kept under static conditions for 1–20 h. After the reaction the solution was transferred to a sealed PTFE flask for hydrothermal treatment at 100 °C for 24 h, followed by filtration and washing with deionized water. All materials were calcinated at 550 °C in order to remove the polymer. The molar ratios for all reagents were P123:HCl:H<sub>2</sub>O:TEOS:heptane: $\text{NH}_4\text{F}$  1:353:10325:60:X:Y, where 16  $\leq X \leq 400$  and 0  $\leq Y \leq 2.74$ . The compositions for the synthesized materials can be seen in the Supporting Information S1.

**Characterization.** Scanning electron microscopy (SEM) was performed with a Leo 1550 Gemini scanning electron microscope operated at 3 kV and a working distance of 3–5 mm. Nitrogen sorption isotherms were obtained with a Micromeritics ASAP 2020 at –196 °C with samples outgassed at 300 °C for 5 h. Pore size distribution was calculated from the adsorption isotherm using the KJS

method<sup>35</sup> and the BET surface area from the relative pressure of 0.06–0.17. It should be noted that the KJS method overestimates the pore size for pores larger than 12 nm.<sup>36</sup> The total pore volume was estimated at  $P_0/P = 0.975$ , and the micropore volume was calculated using the t-plot method in a fitted thickness range of 0.35–0.50 nm. Transmission electron microscopy (TEM) was performed with a FEI Tecnai G2 TF 20 UT microscope operated at 200 kV. TEM samples were prepared by dispersing the product in acetone and depositing it on a hollow carbon grid. Small-angle X-ray scattering (SAXS) measurements were performed on an Empyrean from PANalytical in transmission mode.

## ■ RESULTS

The materials presented here are mainly in a rod or platelet morphology. Our definition is that a platelet is wider than it is high, and the particle height or length is always defined in the direction of the pores. The nomenclature used to describe the particles is defined in Figure 1.

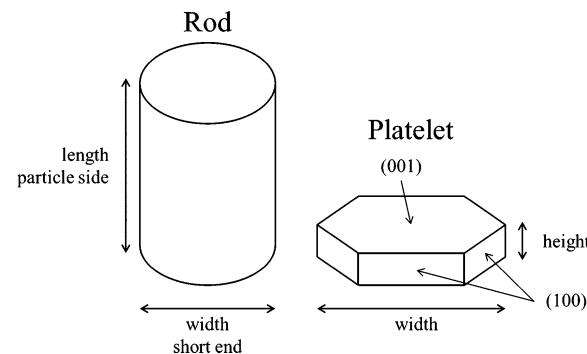


Figure 1. Nomenclature used to describe the particles.

**Heptane Variation.** The particle length increases with the heptane concentration for heptane to P123 molar ratios  $\leq 100$ . For a heptane to P123 molar ratio of 16, the particle length is only  $\sim 300$  nm as seen in Figure 2, while rods synthesized with

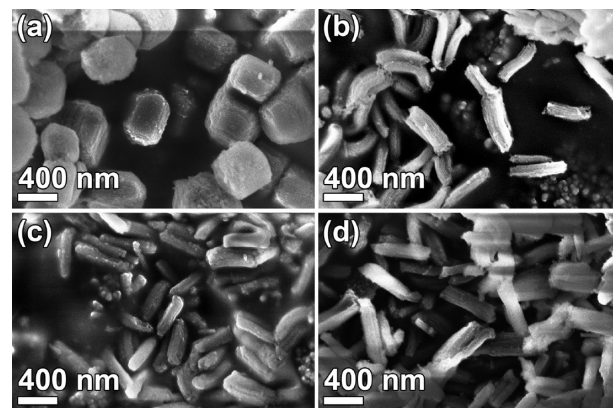


Figure 2. Scanning electron micrographs of mesoporous silica particles synthesized with a heptane to P123 molar ratio of (a) 16, (b) 50, (c) 100, and (d) 400.

a ratio of 400 are almost twice as long. The particle sizes for materials synthesized with different amounts of heptane were determined from SEM micrographs, and the values are presented in Figure 3. It can be seen in both Figure 2 and Figure 3 that the particles elongate and become narrower when the heptane top P123 molar ratio is increased from 16 to 100. At higher heptane concentrations, an increase in heptane

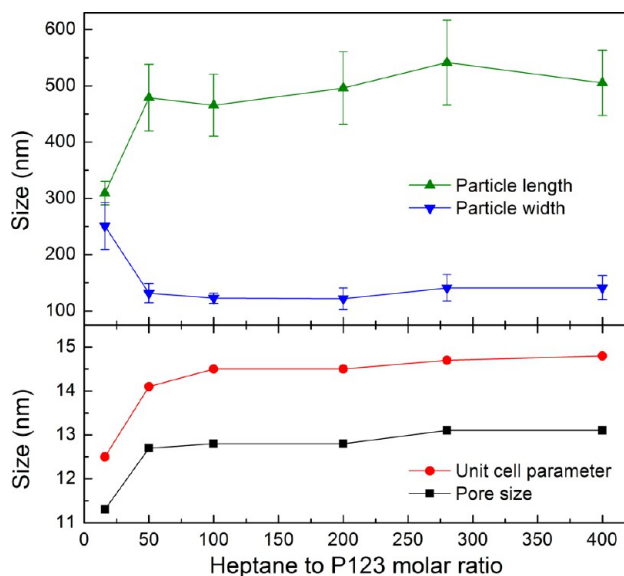


Figure 3. Trends for size parameters for samples synthesized with various heptane concentrations.

amount does not affect the particle dimension to a large extent. Also, the pore size and unit cell parameter show a similar trend where a plateau value is reached at a ratio of 100 and then increases just slightly for higher heptane concentrations. Physisorption isotherms, pore size distributions, and SAXS diffractograms for these samples are shown in Supporting Information S2. All samples display type IV isotherms with type 1 hysteresis loops in the physisorption measurements and three well-resolved peaks in SAXS, indicating hexagonally ordered cylindrical pores as expected for this type of material. As a reference, a sample synthesized without any heptane was produced. This is presented in Supporting Information S3. As shown there, the particles consist of spheres of irregular sizes and contain an unordered porosity and aggregates of small particles; i.e., an ordered material cannot be synthesized with this process without a swelling agent.

**HCl and Cl<sup>-</sup> Variation.** Two syntheses with HCl to P123 molar ratios of 324 and 382 and a heptane to P123 ratio of 16 were performed and the resulting products are presented in Figure 4. The resulting materials show a narrowing of the particle width from  $250 \pm 60$  nm for the low HCl concentration to  $150 \pm 30$  nm for the higher concentration.

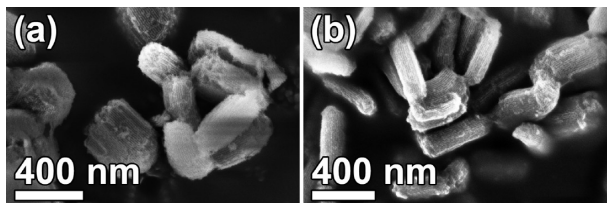


Figure 4. Rods synthesized with a HCl to P123 molar ratio of (a) 324 and (b) 382 and a molar ratio of heptane to P123 equal to 16.

This is in accordance with a previous study when a heptane to P123 molar ratio of 280 was used where this effect was attributed to the change in pH when the HCl concentration was altered.<sup>30</sup>

In order to validate that the shape change is due to pH and not to variations in the chloride ion concentration, Cl<sup>-</sup> was

added to the synthesis solution in the form of NaCl. The lowest HCl to P123 molar ratio (324) was used and the total Cl<sup>-</sup> molar ratio was then increased to 353 and 382 by the salt addition. The syntheses were performed with two amounts of heptane: one heptane to P123 molar ratio of 16 and one of 400. The resulting particles can be seen in Figure 5, where the

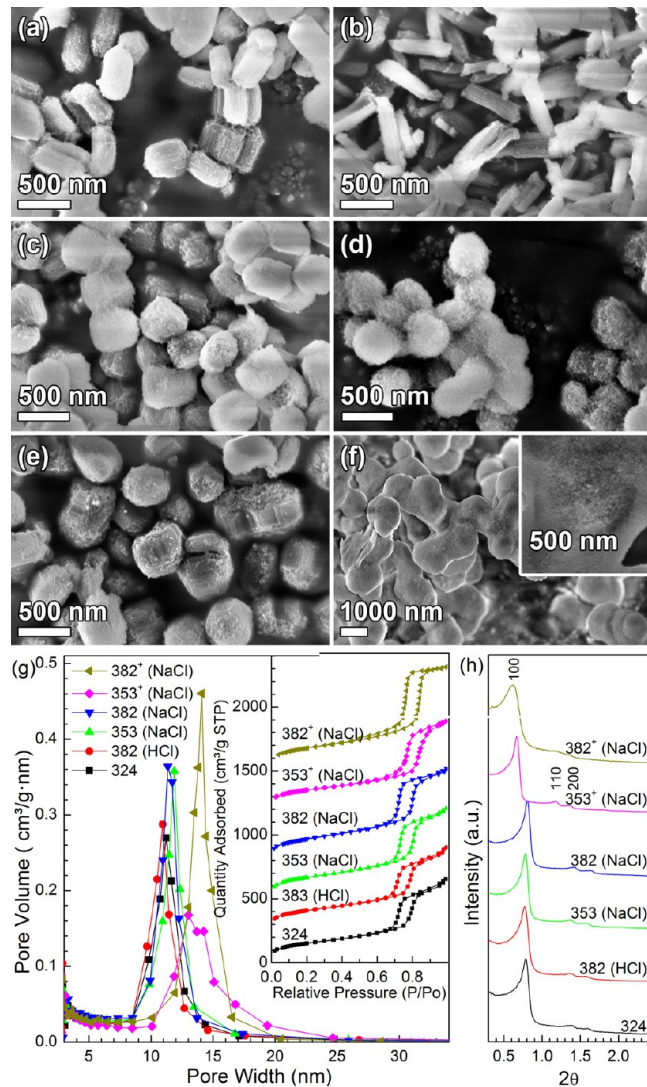
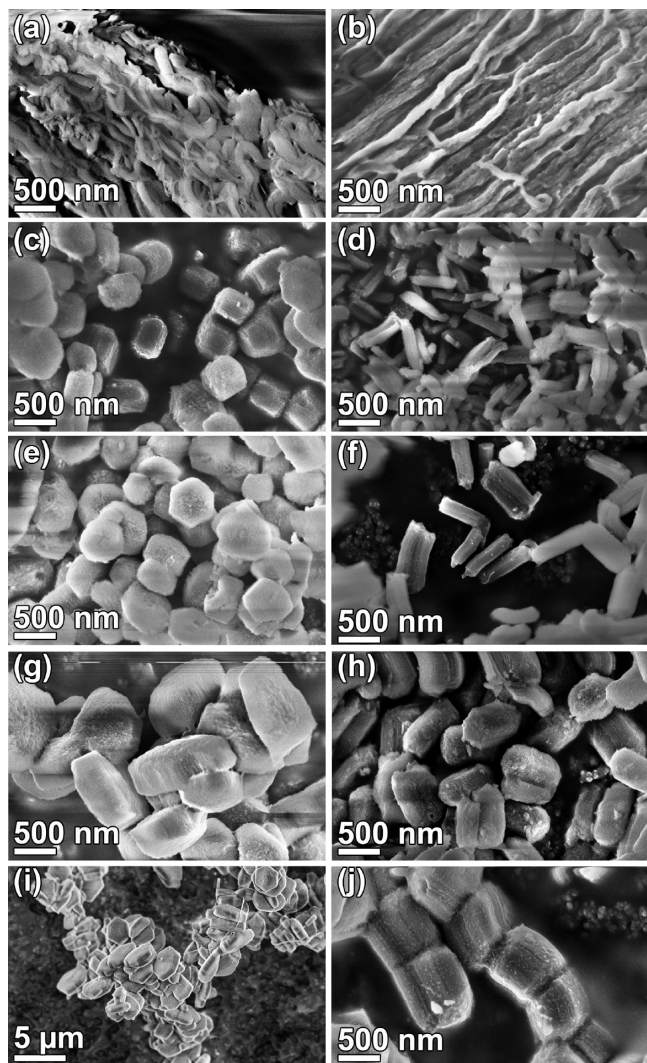


Figure 5. SEM micrographs of materials synthesized with Cl<sup>-</sup> to P123 molar ratios of (a, b) 324, (c, d) 353, and (e, f) 382, where the Cl<sup>-</sup> amount above 324 originates from NaCl; and a heptane to P123 molar ratio of (first column) 16 and (second column) 400, (g) their physisorption isotherms and pore size distributions; and (h) SAXS diffractograms. \*Indicates a heptane to P123 molar ratio of 400.

particles are synthesized with no salt (a, b) and a NaCl to P123 molar ratio of 29 in (c, d) and 58 in (e, f). The result shows that the particles do not elongate upon addition of Cl<sup>-</sup>. For the samples synthesized with a heptane to P123 molar ratio of 16, the particles instead widen from  $280 \pm 40$  nm when the salt is added (see Figure 5, first column). As shown in the second column, the addition of NaCl disturbs the formation of the particles and rounded particles  $\sim 280$  nm wide are formed, and for the highest salt amount the particles are aggregated and disordered as the heptane to P123 molar ratio is increased to 400.

The pore size and unit cell parameter are increasing with increasing  $\text{Cl}^-$  concentration, which can be seen in Figure 5g,h and Supporting Information S1. All samples give type IV isotherms with type 1 hysteresis loops, indicating cylindrical pore typical for this type of material. The ordering is confirmed by the three peaks from SAXS, except for the material synthesized at a heptane to P123 molar ratio of 400 and the highest amount of NaCl, which only gives one peak and one broad feature in the diffractogram. This material is also the material with disordered morphology (see Figure 5f).

**NH<sub>4</sub>F Variation.** Reducing the NH<sub>4</sub>F concentration significantly increases the width of the particles, which can be seen in Figure 6. It is clear from the micrographs that a decrease



**Figure 6.** Samples synthesized with a NH<sub>4</sub>F to P123 molar ratio of (a, b) 2.74, (c, d) 1.83, (e, f) 0.91, (g, h) 0.45, and (i, j) 0 mg of NH<sub>4</sub>F and (first column) 16 and (second column) 400 in heptane to P123 molar ratio. (i) and (j) are synthesized using 1200 min of static time and the other materials with 60 min.

of the NH<sub>4</sub>F concentration in the solution increases the particle width considerably, independent of the heptane amount. The particle length is however constant for each heptane volume, ~300 nm for a heptane to P123 molar ratio of 16 and ~500 nm for a ratio of 400, and the salt is only affecting the particle width morphology wise. An illustration of the particle sizes depending

on the NH<sub>4</sub>F concentration is presented in Supporting Information S4. Even samples synthesized with no salt (Figure 6i,j) follow the trend with increasing particle width. It should though be noticed that those samples have been synthesized with 1200 min of static time. When no salt and 60 min of static time are used, smaller spherical particles are formed (see Supporting Information S5). This indicates that the material is formed slower when no or small amounts of NH<sub>4</sub>F are used.

When the NH<sub>4</sub>F to P123 molar ratio exceeds 1.83, the particles are no longer separated but form elongated fibers, as can be seen in Figure 6a,b. The crystallites in the fibers are thin, and they contain only a few micelles each, especially when high concentrations of heptane are used, which does not give three well-resolved diffraction peaks (see Figure 7d). The physisorption isotherm from this sample, shown in Figure 7b, indicates high external texture. It is seen in the physisorption isotherms that the pore structure is more affected by the salt concentration when a high amount of heptane is used.

There is a slight decrease in pore size with decreasing NH<sub>4</sub>F concentration, which can be seen in Figure 7 and Supporting Information S1. All samples have a hexagonal pore structure, except for the one synthesized with molar ratios of heptane to P123 = 400 and NH<sub>4</sub>F to P123 = 2.74, which is evident from the three diffraction peaks for each material in Figure 7. There is no obvious trend in the unit cell parameter changes upon alterations in the NH<sub>4</sub>F concentration. In this figure, the results from the samples synthesized without any salt and a static time of 60 min are also included. These samples do not contain any ordered mesoporosity but are similar to the results gained from samples collected in the early stages of the formation process (see Figure 9).

**Formation of Platelets and Rods.** Scanning and transmission electron micrographs revealing the formation of platelets are seen in Figure 8. The formation of this material differs from the formation of the ordinary SBA-15 where spherical micelles elongate to cylinders and then aggregate to the hexagonal structure.<sup>37–40</sup> By looking at the SEM micrographs in Figure 8a–j, it is seen that a static time of 5 min (Figure 8a) yields irregular particles in large agglomerations. When the static time is increased, the agglomerates become smaller and more defined, and at a static time of 20 min (Figure 8d) all particles are about 100 nm in size. Larger particles with ordered cylindrical pores are present after a static time of 30 min (Figure 8f). The larger particles grow at the expense of the smaller particles, and after 60 min of static time (Figure 8h), separate platelets ~200–300 nm high are formed. The discrete particles are broadened with time until they reach their final size, i.e. ~950 nm broad after 120 min of static time (Figure 8i,j). The TEM micrographs in Figure 8k–t reveal the evolution on the mesoscale. In Figure 8k it is seen that the large irregular particles consist of porous foam. Each sphere consists of two concentric silica walls. At a static time of 15 min (Figure 8m), short elongated particles are starting to form, and the round particles become larger in size. There are also more layers in the spherical particles, forming an onion-like structure, similar to a MLV.<sup>41</sup> As seen in Figure 8o, rod-like particles have started to form after 30 min of static time. In Figure 8g,p, it is clearly seen that the onion-like structures are preferably positioned on the (001) surface of the platelets. After 50 min of static time, the platelets are formed, but fragments of the decomposed onion-like structures can be seen on the surface of the platelets, which is revealed in Figure 8r. After 60 min, there

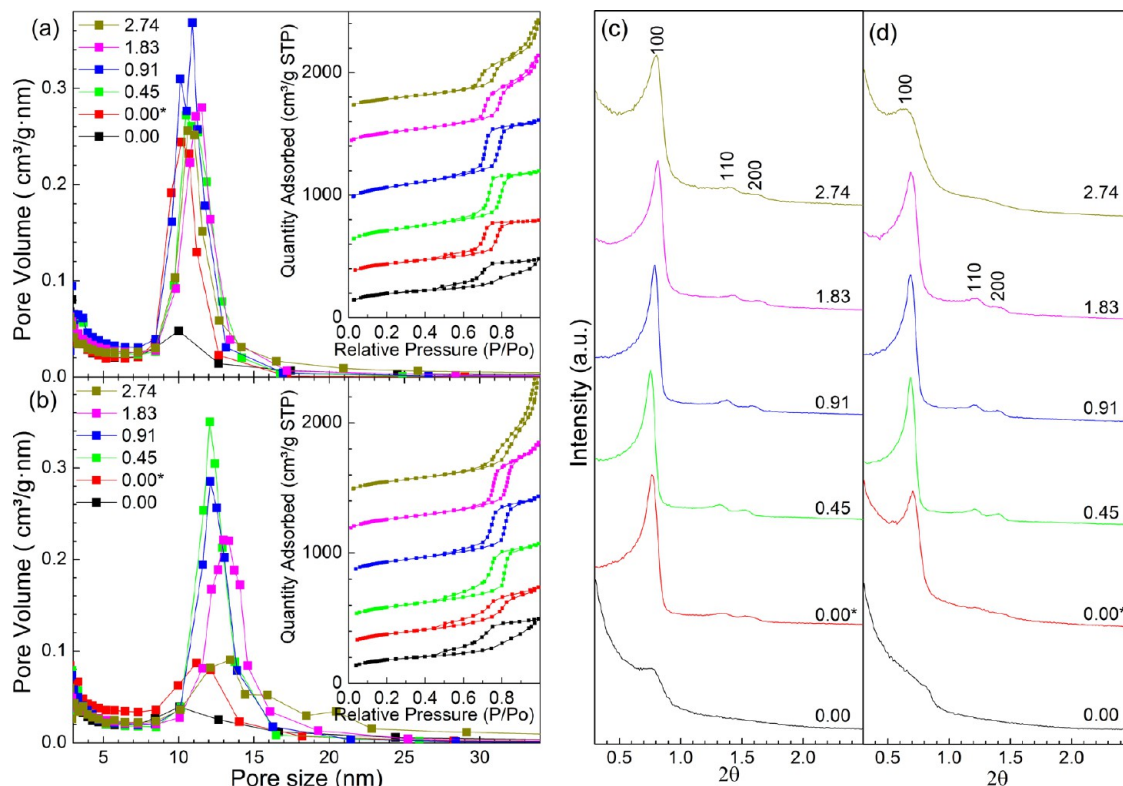


**Figure 7.** (a, b) Pore size distributions and physisorption isotherms and (c, d) SAXS diffractograms for samples synthesized with heptane to P123 molar ratios of (a, c) 16 and (b, d) 400 and various amounts of  $\text{NH}_4\text{F}$ . Asterisk indicates that 1200 min of static time was used.

are no such structures left on the (001) surface of the platelets and the hexagonal order of the pores is apparent (Figure 8s,t).

The formation of cylindrical pores after 20 min is verified by the physisorption data in Figure 9a. As seen in the pore size distributions, there are no mesopores present in the material for materials synthesized with a static time less than 20 min. After 20 min, there are cylindrical mesopores present, as confirmed by the isotherms. The size of these mesopores is decreasing from 13.2 to 9.8 nm with increasing static time. The evolution of the ordered material is also confirmed by the SAXS diffractograms in Figure 9c, in which it is seen that the material synthesized with static times above 30 min gives three well-resolved peaks, corresponding to the 100, 110, and 200 reflections of the hexagonal  $p6mm$  structure, typical for this type of material. Data from these measurements are presented in Table 1. For the material synthesized with 30 min of static time, there is only one peak, indicating that order starts to occur in the material. For samples synthesized with a shorter static time, there are no clear peaks and only a broad weak hump that indicates some but weak pore ordering in the material. These results correspond well with the TEM micrographs in Figure 8k–t.

Rods synthesized with the same amount of heptane but a  $\text{NH}_4\text{F}$  to P123 molar ratio of 1.83 and 5 min of static time are seen in Figure 9e. As seen in the figure, the rod morphology is formed within 5 min of static time, which is consistent with previously reported data for this morphology.<sup>30</sup> Also here, the pore size and unit cell parameter are decreasing during the first 30 min of static time and even after the final morphology is reached (see Figure 9b,d and Table 1).

## ■ DISCUSSION

**Heptane.** Heptane is clearly affecting the particle size and the mesoscopic structure of the material. The effect is though more pronounced for low amounts of heptane (cf. Figures 2 and 3). This is due to the solubility of heptane and TEOS. Theoretical calculations have shown that the solubilization capacity of heptane in PEO–PPO blocks is 0.567 mmol per gram of hydrophobic block at 25 °C.<sup>42</sup> This should in our case correspond to a heptane to P123 molar ratio of 3.3. However, this prediction does not account completely for the conditions in our synthesis, i.e., pH, salt addition, and TEOS presence. A study of a similar system, including  $\text{NH}_4\text{F}$  and using decane instead of heptane, shows an increasing pore size with decane content up to a decane to P123 molar ratio of 70;<sup>31,32</sup> i.e., at this ratio, the micelles are saturated with decane. It is known that the solubilization of hydrocarbons in this type of surfactant increases with decreasing hydrocarbon chain length.<sup>42,43</sup> From our results shown in Figure 3, it is clear that the particle morphology and mesoscopic structure are most affected by variations in heptane to P123 molar ratio up to 100. Most probably, for the lowest heptane amounts, all heptane/TEOS mixture goes into the micelles and expands them. The formation of particles with a heptane to P123 molar ratio of 16 will be discussed in detail later. While for larger heptane amounts (heptane to P123 molar ratio >50), oil droplets will form in the solution and not affect the micelles further and hence not affect the particle morphology.

The effects of changing synthesis parameters are larger when small amounts of heptane are used. This can be due to the solubilization of TEOS in heptane or if the heptane is solubilized in the TEOS. For the low heptane amounts, the TEOS is mostly present in the aqueous environment and

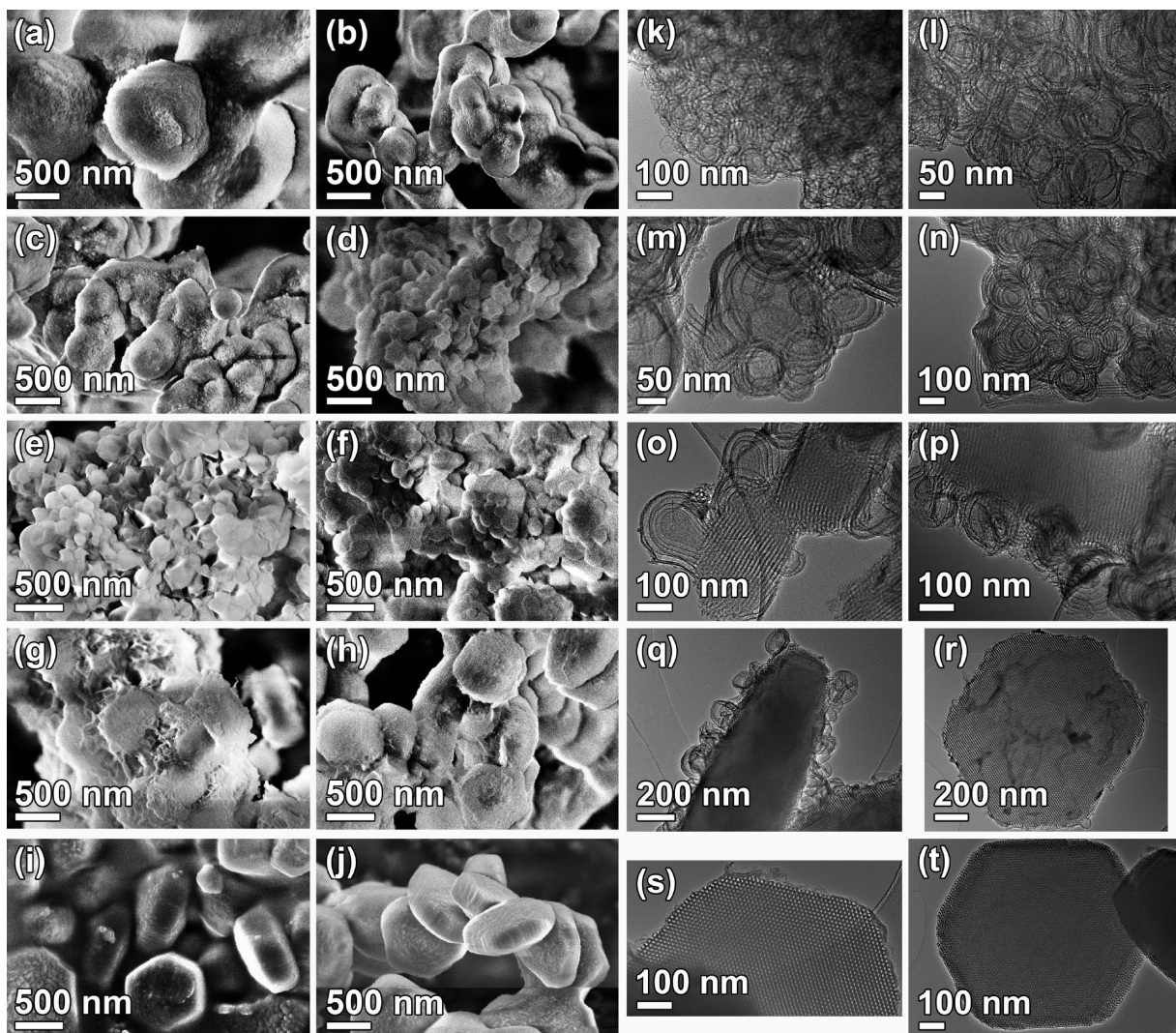


**Figure 8.** Scanning electron micrographs of samples synthesized with  $\text{NH}_4\text{F}$  to P123 and heptane to P213 molar ratios of 0.45 and 16, respectively, and (a) 5, (b) 10, (c) 15, (d) 20, (e) 30, (f) 40, (g) 50, (h) 60, (i) 120, and (j) 1200 min of static time and transmission electron micrographs of samples with (k) 5, (l) 10, (m), 15, (n), 20, (o, p) 30, (q) 40, (r) 50, (s) 60, and (t) 1200 min of static time.

therefore easily affected. When larger concentrations of heptane are used, all TEOS is solubilized in the oil and hence shielded from alterations in the aqueous environment. The plateau for the shape and mesoscopic structure is actually reached when the volume of TEOS is similar to the volume of heptane, since a heptane to P123 molar ratio of 50 in our case corresponds to 6 mL of heptane, and above this heptane concentration the particle shape and mesoscopic values are constant.

**HCl and  $\text{Cl}^-$ .** The particle size is affected by pH in such a way that a high HCl concentration results in narrow rods, with narrow pores, which is in accord with previous observations.<sup>30</sup> The effect was attributed to a competition between the increased formation rate due to lower pH and the decrease of  $\text{F}^-$  due to the formation of HF. In the present study with less heptane, the particles have an even pore length, even at the lowest HCl amount. TEOS is less diluted when a heptane to P123 molar ratio of 16 is used, compared to a ratio of 280 in the previous study, which facilitate a more rapid hydrolysis of TEOS. The micelles are then given more time to elongate before they aggregate to form the hexagonal structure, and hence they all have the same length. A higher hydrolysis rate also results in formation of more seeds, at the higher HCl

concentration. Since the aggregation of micelles tends to be side by side more narrow, rods are formed when the number of seeds is increased for a given concentration of TEOS.

The decreasing pore size is due to the effect of reducing the amount of  $\text{F}^-$ , since the fluoride ions are acting as catalyst for the hydrolysis and condensation of TEOS.<sup>44–46</sup> For high concentrations of  $\text{F}^-$ , the silica oligomers form networks that cannot penetrate deep into the PEO shell of the micelles.<sup>47</sup> When the amount of  $\text{F}^-$  is decreased, smaller oligomers will form which can go deeper into the PEO shell. This will yield particles with smaller pore sizes, which is consistent with the results seen in Figure 7 and Supporting Information S1.

In order to determine that in fact it is the HCl and  $\text{F}^-$  that affect the particle shape and not the ionic strength in the solution from  $\text{Cl}^-$ , samples with additions of NaCl were synthesized. From the micrographs in Figure 5a–e it is obvious that increasing the  $\text{Cl}^-$  concentration does not narrow the rod; instead, they become wider independent of the heptane amount. The pore order is well retained for the samples synthesized with low heptane concentration but starts to disorder when the higher amount of heptane is used (see Figure 5h). NaCl is regarded to be a salting-out salt, affecting

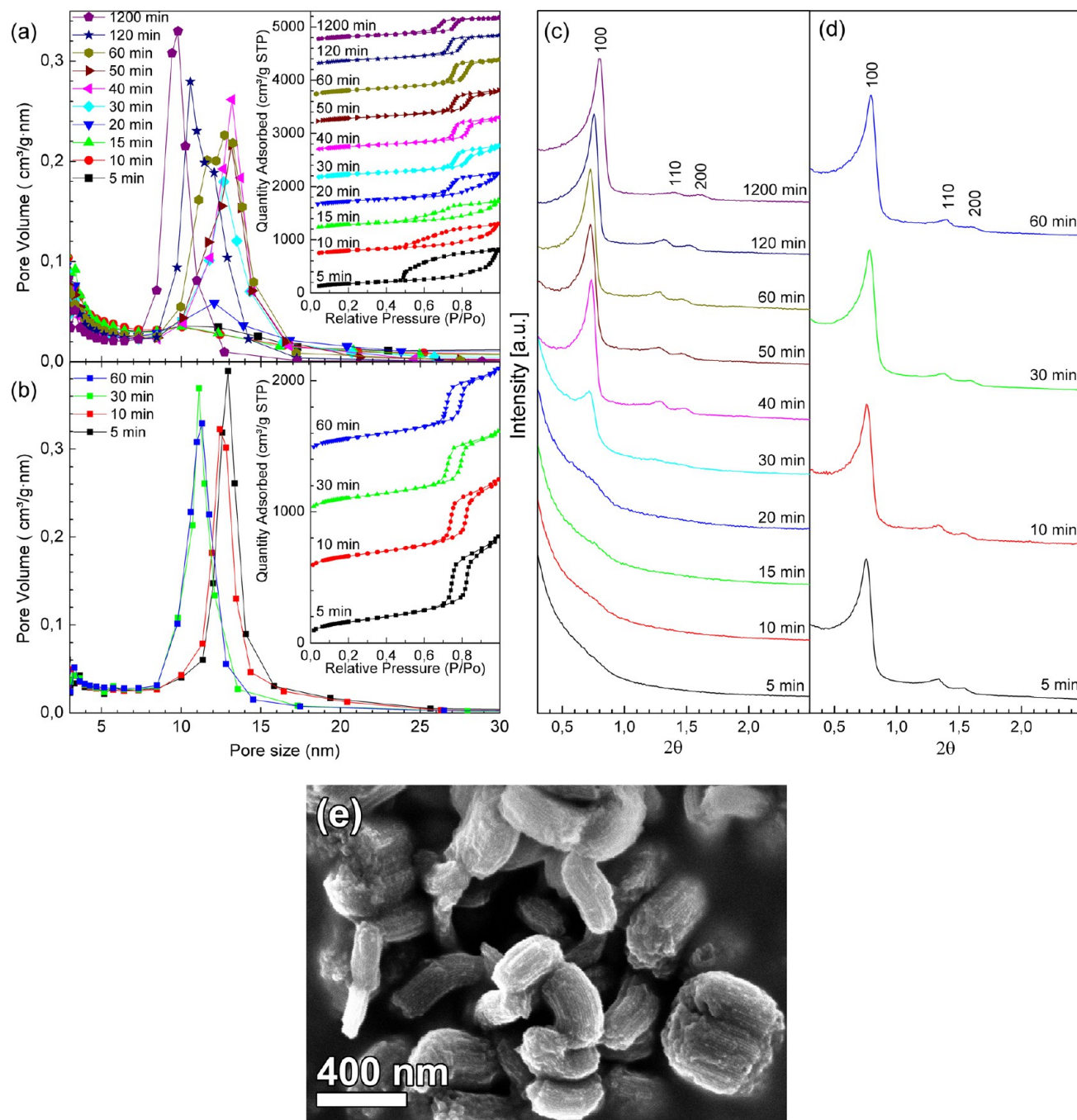


**Figure 9.** Pore size distributions and physisorption isotherms and SAXS diffractograms for samples synthesized with  $\text{NH}_4\text{F}$  to P123 molar ratios of (a, c) 0.45 and (b, d) 1.83, a heptane to P123 molar ratio of 16, and variations in the static time, and (e) rods synthesized with molar ratios of heptane and  $\text{NH}_4\text{F}$  to P123 equal to 16 and 1.83, respectively, and 5 min of static time.

the solubility of P123.<sup>48</sup> It also increases the reaction rate and can drive the silica condensation to become more complete.<sup>49</sup> Both these effects have an impact on the morphology of the particle, and similar results have been seen when Zr ions with equivalent properties to NaCl have been used.<sup>24</sup>

**NH<sub>4</sub>F.** The particle width is clearly affected by the  $\text{NH}_4\text{F}$  concentration, as is seen in Figure 6. In order to elucidate if the shape change stems from  $\text{F}^-$  or  $\text{NH}_4^+$  ions, samples were prepared with an alternate  $\text{NH}_4^+$  source. A mixture with a  $\text{NH}_4\text{F}$  to P123 molar ratio of 0.45 was used as a starting crude to which  $\text{NH}_4\text{Cl}$  was added such that the total  $\text{NH}_4^+$  to P123 molar ratio became 0.91 or 1.83. The SEM micrographs in

Supporting Information S6 show that there is no morphological change in these samples compared to what is seen in Figure 6g, i.e., when no additional  $\text{NH}_4\text{Cl}$  is used. Hence, we conclude that  $\text{F}^-$  solely is responsible for the change in morphology.

Also, the pore shape is slightly affected by the  $\text{F}^-$  concentration (see Figure 7). The samples with ordered pore morphology show a tail developing in the hysteresis loops when the ion concentration is decreased. This is an indication of a tissue phase in between the mesoporous particles or, more probably, that the pores have not completely evolved to their final cylindrical shape and still contain constrictions<sup>50</sup> of silica due to incomplete condensation of TEOS within the pores.

**Table 1.** Physisorption Data and Unit Cell Parameters for Samples Synthesized with a Heptane to P123 Molar Ratio of 16 and Variations in the Static Time

NH <sub>4</sub> F/P123	static time (min)	specific surface area [m <sup>2</sup> /g]	pore volume [cm <sup>3</sup> /g]	micropore volume [cm <sup>3</sup> /g]	pore size [nm]	unit cell parameter [nm]
0.45	5	624	1.27	0.041		
	10	643	1.06	0.036		
	15	669	1.00	0.028		
	20	674	1.10	0.043		
	30	662	1.13	0.036	12.7	14.2 <sup>a</sup>
	40	648	1.12	0.034	13.2	13.9
	50	688	1.12	0.049	13.1	14.0
	60	721	1.21	0.033	12.7	14.1
	120	656	1.02	0.034	10.6	13.5
	1200	628	0.82	0.058	9.8	12.8
	1.83	577	1.25	0.018	12.9	13.4
	10	580	1.16	0.028	12.5	13.3
	30	557	1.03	0.026	11.2	12.9
	60	580	1.08	0.022	11.3	12.8

<sup>a</sup>Calculated from the 100 peak only.

The formation study (Figures 8 and 9 and Table 1) reveals that the particles synthesized with higher F<sup>-</sup> concentrations form faster due to the catalytic effect of the fluoride ions. The pore evolution and unit cell are though decreasing during the first hour (see Table 1) due to condensation of silica in the structure.<sup>37,51</sup> The time scale for formation of platelets, i.e., for samples with a NH<sub>4</sub>F to P123 molar ratio of 0.45, is however significantly longer. They reach their final morphology first after 2 h of static time, and the decrease in pore size and unit cell parameter continues up to 20 h after turning off the stirring.

In order to establish if the reaction rate is affecting the particle morphology, the syntheses yielding short rods and platelets were repeated using TMOS instead of TEOS. TMOS has faster hydrolysis and condensation rates,<sup>52</sup> and hence the particles would be narrower if the gelation time was the key parameter for variations in particle width. As can be seen in Supporting Information S7c,d, the particles synthesized with TMOS are not narrower compared to the materials synthesized using TEOS; they are rather broadened from 250 to 320 nm when the low heptane concentration is used and from 950 to 1200 nm for the higher concentration. A similar effect has been seen when Zr ions have been added to SBA-15 syntheses which also increases the reaction rate.<sup>24</sup>

Both additions of F<sup>-</sup> and variations of the silica precursor affect the balance between the hydrophobic and hydrophilic part of the surfactants. The particle length is unaffected by these alterations, but the particle width is greatly affected.

Several studies have previously shown syntheses where platelets have been observed, but the explanations for why the platelets formed have varied. Morphological changes of SBA-15 particles were observed when variation in synthesis temperatures and P104 was used as the surfactant.<sup>22,53,54</sup> In that case, a lower reaction temperature favored side by side attachment of the particles, and an increase in temperature yielded rod and fiber like structures. Furthermore, Linton et al. showed that the aggregation manner of the particles, i.e., if the particles aggregated or not, was affected by salt additions during the synthesis.<sup>54</sup> In a system similar to ours, platelet morphologies could be formed when the TEOS to P123 ratio was increased from 60 to 77.<sup>31</sup> We propose that the key to the formation of platelets is the size of the micelle corona. All the reported parameters observed to influence the formation of platelets, temperature, salt, and TEOS affect the PEO corona of the

micelles. The PEO are less soluble in water when the temperature is increased;<sup>55</sup> salts containing salting-out ions, e.g., F<sup>-</sup>, Br<sup>-</sup>, and NH<sub>4</sub><sup>+</sup>, are also decreasing the solubility of PEO chains.<sup>56</sup> An increase in TEOS concentration will also yield a larger corona due to the increased number of silica oligomers. Another observation is that it seems to be easier to synthesize a platelet morphology using P104 instead of P123. P104 has a larger fraction of PEO compared to P123 and hence longer PEO chains. Combining these observations, it is clear that longer available PEO chains, i.e., a larger corona, favor the formation of wider particles, e.g., platelets. The longer chains entangle more easily, and when they are silicated, it is simple for other micelles and particles to attach and grow to larger aggregates. Hence, larger available PEO domains lead to side by side attachment and a broadening of the particles.

The effect of F<sup>-</sup> can also be observed in the pore size of the material, where a decreased ion content leads to smaller pore sizes (see Figure 7 and Supporting Information S1). As previously mentioned, the fluoride ions hydrolyze TEOS by a nucleophilic attack<sup>45</sup> and large oligomers are formed. These oligomers cannot penetrate deep into the corona of the micelles, leading to thinner silica walls and larger pores of the calcined material. A lower fluoride ion concentration yields a slower hydrolysis and condensation and, hence, smaller silica oligomers that can go deeper into the micelles and thereby decrease the pore size.

**Formation of Platelets and Rods.** The results in Figures 8 and 9 as well as Table 1 all reveal that the platelets are formed under a period of 120 min of static time. The pore size and wall thickness are though still evolving during 1200 min due to silica condensation<sup>37,51</sup> (see Table 1). This can be compared with the formation of rods in a similar system, where the morphology is formed within 5 min of static time, but the pore size and wall thickness evolve for 30 min.<sup>30</sup>

In our platelet system (NH<sub>4</sub>F to P123 molar ratio of 0.45) there is after 5 min of static time no order in the material, which consists of a sponge-like structure of aggregated silica spheres. The spheres grow in size with time and add layers of silica shells around them, forming MLVs. The MLVs opens up and elongate, and particles with ordered cylindrical pores start to appear after a static time of 15 min and are apparent after 30 min (see Figure 8m-p). It should be noted that in this study the material has undergone hydrothermal treatment after the

static time, and in this step the material can change its morphology before quenching of the structure by condensation of silica on the micelles.

It is clear from Figure 8f,p,q that the MLVs preferably attach to the (001) surface of the platelets. This should be due to the difference in surface energy and hydrophilicity between the (100) and (001) surfaces of the platelets. At the (001) surface micellar caps are present and the surface is more hydrophobic. Since the MLVs contain droplets of heptane, they prefer this surface of the particle. After 60 min, the particles are well separated and the platelet morphology is clearly visible, as seen in Figure 8h,s, even though the particles continue to form so that they all get the same size and shape which is reached after 1200 min.

The particle evolution seen here is similar to observations made when the reaction temperature is varied in similar systems with decane<sup>41</sup> and undecane.<sup>57</sup> There, phase transformations from a swollen inverse hexagonal phase ( $H_2$ ) to a swollen lamellar phase ( $L_\alpha$ ) and finally to a swollen normal micelle phase ( $L_1$ ) were seen when the reaction temperature was increased. It has been suggested that MLVs are formed from  $L_\omega$  which upon shearing organizes into spherical MLVs<sup>58</sup> in which the nanoscopic channels of water are partitioned by, in their case, decane.<sup>41</sup> The layers of silica are formed upon condensation of the TEOS confined within the compartments of aqueous nanochannels. It should be noted that the observed MLVs in our study are seen in a hydrothermally treated sample. Hence, it is most probable that the  $L_\alpha$  phase is present during the formation of our platelets and that this phase then evolves further to the hexagonal  $H_1$  phase.

It is well-known that the micelle structure depends on the relation between hydrophilic and hydrophobic parts of the surfactant, i.e., the packing parameter. The phase transformation observed upon variations in the reaction temperature is due to the shift in hydrophilicity of the PEO chains of the P123 and the solubility of alkanes in the PPO moieties.<sup>57</sup> During the formation of our particles, the reaction temperature is kept constant, but the micelles undergo several steps during the formation of the final material. The formation of SBA-15 has been well studied, and the most common view when P123 is used as the surfactant is that spherical micelles are elongated into worm-like micelles, which then aggregate into the hexagonal structure.<sup>37–40</sup> In our case, the system is more complex due to the presence of heptane and  $\text{NH}_4\text{F}$ . The formation of systems including swelling agents, such as TMB, has recently been studied with SAXS and SANS, and even though the micelles are significantly swollen by TMB, there have not been any alterations from the conventional formation route regardless of reaction temperature.<sup>59,60</sup> Hence, the different formation route seen in the present system must be due to the combination of low temperature, excess heptane in the form of oil droplets in the solution, and  $\text{NH}_4\text{F}$ .

The continued evolution of the pore size and unit cell parameter (Figure 9 and Table 1) during static times longer than 60 min is due to continuous condensation within the pore walls.<sup>38</sup> The trend with decreasing pore size and unit cell parameter is apparent for both platelets and rods.

## CONCLUSIONS

We have shown that it is possible to tune the shape of separate mesoporous silica particles in a low-temperature synthesis with additions of heptane and  $\text{NH}_4\text{F}$ . The rod morphology can be synthesized with a broad range of heptane concentrations, and

the rod length, width, and mesoscopic structure are dependent on the solubilization of heptane in the micelles. A decrease in pH narrows the rods independent of heptane concentration. Additionally, the particles are broadened by decreasing the  $\text{NH}_4\text{F}$  concentration independent of heptane amount, and platelets can be formed, both with low amounts of  $\text{NH}_4\text{F}$  or without the salt. This broadening originates from the decrease in fluoride ion concentration and not the increased hydrolysis and condensation rates of TEOS as was confirmed by exchanging the silica precursor to TMOS. A mechanism for the particle broadening, where side by side attachment of particles due to the availability of PEO chains in P123 occurs, is suggested. Furthermore, the platelets have a slower formation rate than rods due to the reduced amount of the fluoride ion catalyst. The formation of platelets is complex and includes a route via MLVs.

## ASSOCIATED CONTENT

### S Supporting Information

Section S1: table with the samples synthesis conditions, their physisorption results, SAXS data, and particle dimensions; section S2: pore size distributions, physisorption isotherms, and SAXS diffractograms for materials synthesized with various amounts of heptane; section S3: (a) SEM, (b) TEM, and (c) results from physisorption for a sample synthesized without heptane; section S4: trends in particle dimensions and mesoscopic properties for materials synthesized with various  $\text{NH}_4\text{F}$  and a heptane to P123 molar ratio of (a) 16 and (b) 400; section S5: SEM micrographs of samples synthesized without  $\text{NH}_4\text{F}$ , a heptane to P123 molar ratio of 16 and 400, and 60 min of static time; section S6: SEM micrographs of samples synthesized with a  $\text{NH}_4\text{F}$  to P123 molar ratio of 0.45 and various  $\text{NH}_4^+$  concentrations; section S7: physisorption isotherms, pore size distributions, SAXS diffractograms, and SEM micrographs of materials synthesized with TMOS and various  $\text{NH}_4\text{F}$  to P123 molar ratios. This material is available free of charge via the Internet at <http://pubs.acs.org>.

## AUTHOR INFORMATION

### Corresponding Author

\*E-mail magod@ifm.liu.se; Ph +46 (0)13 28 29 96; Fax +46 (0) 13 28 89 18 (M.O.).

### Notes

The authors declare no competing financial interest.

## ACKNOWLEDGMENTS

The Swedish Research Council (VR), Linnaeus environment LiLi-NFM, and Nanolith Sverige AB are acknowledged for financial support.

## REFERENCES

- (1) Cauda, V.; Mühlstein, L.; Onida, B.; Bein, T. Tuning Drug Uptake and Release Rates through Different Morphologies and Pore Diameters of Confined Mesoporous Silica. *Microporous Mesoporous Mater.* **2009**, *118*, 435–442.
- (2) Rosenholm, J. M.; Sahlgren, C.; Lindén, M. Towards Multifunctional, Targeted Drug Delivery Systems using Mesoporous Silica Nanoparticles - Opportunities & Challenges. *Nanoscale* **2010**, *2*, 1870–1883.
- (3) Gu, J.; Shi, J.; Xiong, L.; Chen, H.; Ruan, M. A New Strategy to Incorporate Highly Dispersed Nanoparticles into the Pore Channels of Mesoporous Silica Thin Films. *Microporous Mesoporous Mater.* **2004**, *74*, 199–204.

- (4) Tsai, H.; Córdoba, J. M.; Johansson, E. M.; Ballem, M. A.; Odén, M. Copper Nanoparticles Synthesized via Electroless Copper Deposition in Sheet-like Mesoporous Type SBA-15. *J. Nanosci. Nanotechnol.* **2011**, *11*, 3493.
- (5) Weng, T.; Tseng, H.; Wey, M. Fabrication and Characterization of Poly(Phenylene Oxide)/SBA-15/Carbon Molecule Sieve Multilayer Mixed Matrix Membrane for Gas Separation. *Int. J. Hydrogen Energy* **2010**, *35*, 6971–6983.
- (6) Song, S.; Liang, Y.; Li, Z.; Wang, Y.; Fu, R.; Wu, D.; Tsikararas, P. Effect of Pore Morphology of Mesoporous Carbons on the Electrocatalytic Activity of Pt Nanoparticles for Fuel Cell Reactions. *Appl. Catal., B* **2010**, *98*, 132–137.
- (7) Zhao, D.; Feng, J.; Huo, Q.; Melosh, N.; Fredrickson, G. H.; Chmelka, B. F.; Stucky, G. D. Triblock Copolymer Syntheses of Mesoporous Silica with Periodic 50 to 300 Angstrom Pores. *Science* **1998**, *279*, 548–552.
- (8) Prieto, G.; Martínez, A.; Murciano, R.; Arribas, M. A. Cobalt Supported on Morphologically Tailored SBA-15 Mesostructures: The Impact of Pore Length on Metal Dispersion and Catalytic Activity in the Fischer-Tropsch Synthesis. *Appl. Catal., A* **2009**, *367*, 146–156.
- (9) Sujandi; Prasetyanto, E. A.; Park, S. Synthesis of Short-Channelled Amino-Functionalized SBA-15 and Its Beneficial Applications in Base-Catalyzed Reactions. *Appl. Catal., A* **2008**, *350*, 244–251.
- (10) Fan, J.; Lei, J.; Wang, L.; Yu, C.; Tu, B.; Zhao, D. Rapid and High-Capacity Immobilization of Enzymes Based on Mesoporous Silicas with Controlled Morphologies. *Chem. Commun.* **2003**, 2140–2141.
- (11) Sun, J.; Zhang, H.; Tian, R.; Ding, M.; Bao, X.; Su, D. S.; Zou, H. Ultrafast Enzyme Immobilization Over Large-Pore Nanoscale Mesoporous Silica Particles. *Chem. Commun.* **2006**, 1322–1324.
- (12) Gustafsson, H.; Johansson, E. M.; Barrabino, A.; Odén, M.; Holmberg, K. Immobilization of Lipase from *Mucor miehei* and *Rhizopus oryzae* into Mesoporous Silica—The Effect of Varied Particle Size and Morphology. *Colloids Surf., B* **2012**, *100*, 22–30.
- (13) Sen Karaman, D.; Desai, D.; Senthilkumar, R.; Johansson, E.; Ratts, N.; Oden, M.; Eriksson, J.; Sahlgren, C.; Toivola, D.; Rosenholm, J. Shape Engineering Vs Organic Modification of Inorganic Nanoparticles as a Tool for Enhancing Cellular Internalization. *Nanoscale Res. Lett.* **2012**, *7*, 358.
- (14) Ma, L.; Zhai, S.; Liu, N.; Zhai, B.; An, Q. Controlled Fabrication and Application of Platelet SBA-15 Materials. *Prog. Chem.* **2012**, *24*, 471–482.
- (15) Yu, C.; Fan, J.; Tian, B.; Zhao, D.; Stucky, G. D. High-Yield Synthesis of Periodic Mesoporous Silica Rods and Their Replication to Mesoporous Carbon Rods. *Adv. Mater.* **2002**, *14*, 1742.
- (16) Sayari, A.; Han, B.; Yang, Y. Simple Synthesis Route to Monodispersed SBA-15 Silica Rods. *J. Am. Chem. Soc.* **2004**, *126*, 14348–14349.
- (17) Schmidt-Winkel, P.; Yang, P.; Margolese, D. I.; Chmelka, B. F.; Stucky, G. D. Fluoride-Induced Hierarchical Ordering of Mesoporous Silica in Aqueous Acid-Syntheses. *Adv. Mater.* **1999**, *11*, 303–307.
- (18) Wang, Y.; Zhang, F.; Wang, Y.; Ren, J.; Li, C.; Liu, X.; Guo, Y.; Guo, Y.; Lu, G. Synthesis of Length Controllable Mesoporous SBA-15 Rods. *Mater. Chem. Phys.* **2009**, *115*, 649–655.
- (19) Ding, Y.; Yin, G.; Liao, X.; Huang, Z.; Chen, X.; Yao, Y.; Li, J. A Convenient Route to Synthesize SBA-15 Rods with Tunable Pore Length for Lysozyme Adsorption. *Microporous Mesoporous Mater.* **2013**, *170*, 45–51.
- (20) Ding, Y.; Yin, G.; Liao, X.; Huang, Z.; Chen, X.; Yao, Y. Key Role of Sodium Silicate Modulus in Synthesis of Mesoporous Silica SBA-15 Rods with Controllable Lengths and Diameters. *Mater. Lett.* **2012**, *75*, 45–47.
- (21) Cui, X.; Moon, S.; Zin, W. High-Yield Synthesis of Monodispersed SBA-15 Equilateral Hexagonal Platelet with Thick Wall. *Mater. Lett.* **2006**, *60*, 3857–3860.
- (22) Linton, P.; Alfredsson, V. Growth and Morphology of Mesoporous SBA-15 Particles. *Chem. Mater.* **2008**, *20*, 2878–2880.
- (23) Jin, Z.; Wand, X.; Cui, X. Synthesis and Morphological Investigation of Ordered SBA-15-Type Mesoporous Silica with an Amphiphilic Triblock Copolymer Template under Various Conditions. *Colloids Surf., A* **2008**, *316*, 27–36.
- (24) Chen, S.; Tang, C.; Chuang, W.; Lee, J.; Tsai, Y.; Chan, J. C. C.; Lin, C.; Liu, Y.; Cheng, S. A Facile Route to Synthesizing Functionalized Mesoporous SBA-15 Materials with Platelet Morphology and Short Mesochannels. *Chem. Mater.* **2008**, *20*, 3906–3916.
- (25) Chen, S.; Huang, C.; Yokoi, T.; Tang, C.; Huang, S.; Lee, J.; Chan, J. C. C.; Tatsumi, T.; Cheng, S. Synthesis and Catalytic Activity of Amino-Functionalized SBA-15 Materials with Controllable Channel Lengths and Amino Loadings. *J. Mater. Chem.* **2012**, *22*, 2233–2243.
- (26) Cao, L.; Kruk, M. Facile Method to Synthesize Platelet SBA-15 Silica with Highly Ordered Large Mesopores. *J. Colloid Interface Sci.* **2011**, *361*, 472–476.
- (27) Kjellman, T.; Reichhardt, N.; Sakeye, M.; Smatt, J.; Lindn, M.; Alfredsson, V. Independent Fine-Tuning of the Intrawall Porosity and Primary Mesoporosity of SBA-15. *Chem. Mater.* **2013**, *25*, 1989–1997.
- (28) Johansson, E. M.; Córdoba, J. M.; Odén, M. Synthesis and Characterization of Large Mesoporous Silica SBA-15 Sheets with Ordered Accessible 18 nm Pores. *Mater. Lett.* **2009**, *63*, 2129–2131.
- (29) Johansson, E. M.; Córdoba, J. M.; Odén, M. The Effects on Pore Size and Particle Morphology of Heptane Additions to the Synthesis of Mesoporous Silica SBA-15. *Microporous Mesoporous Mater.* **2010**, *133*, 66–74.
- (30) Johansson, E. M.; Ballem, M. A.; Córdoba, J. M.; Odén, M. Rapid Synthesis of SBA-15 Rods with Variable Lengths, Widths, and Tunable Large Pores. *Langmuir* **2011**, *27*, 4994–4999.
- (31) Zhang, H.; Sun, J.; Ma, D.; Weinberg, G.; Su, D. S.; Bao, X. Engineered Complex Emulsion System: Toward Modulating the Pore Length and Morphological Architecture of Mesoporous Silicas. *J. Phys. Chem. B* **2006**, *110*, 25908–25915.
- (32) Zhang, H.; Sun, J.; Ma, D.; Bao, X.; Klein-Hoffman, A.; Weinberg, G.; Su, D.; Schlogl, R. Unusual Mesoporous SBA-15 with Parallel Channels Running along the Short Axis. *J. Am. Chem. Soc.* **2004**, *126*, 7440–7441.
- (33) Han, Y.; Ying, J. Y. Generalized Fluorocarbon-Surfactant-Mediated Synthesis of Nanoparticles with Various Mesoporous Structures. *Angew. Chem., Int. Ed.* **2005**, *44*, 288–292.
- (34) Gao, F.; Botella, P.; Corma, A.; Blesa, J.; Dong, L. Monodispersed Mesoporous Silica Nanoparticles with Very Large Pores for Enhanced Adsorption and Release of DNA. *J. Phys. Chem. B* **2009**, *113*, 1796–1804.
- (35) Kruk, M.; Jaroniec, M.; Sayari, A. Application of Large Pore MCM-41 Molecular Sieves to Improve Pore Size Analysis Using Nitrogen Adsorption Measurements. *Langmuir* **1997**, *13*, 6267–6273.
- (36) Jaroniec, M.; Solocyoc, L. A. Improvement of the Kruk-Jaroniec-Sayari Method for Pore Size Analysis of Ordered Silicas with Cylindrical Mesopores. *Langmuir* **2006**, *22*, 6757–6760.
- (37) Ruthstein, S.; Schmidt, J.; Kesselman, E.; Telmon, Y.; Goldfarb, D. Resolving Intermediate Solution Structures during the Formation of Mesoporous SBA-15. *J. Am. Chem. Soc.* **2006**, *128*, 3366–3374.
- (38) Zholobenko, V. L.; Khodakov, A. Y.; Impérator-Clerc, M.; Durand, D.; Grillo, I. Initial Stages of SBA-15 Synthesis: An Overview. *Adv. Colloid Interface Sci.* **2008**, *142*, 67–74.
- (39) Imperator-Clerc, M.; Grillo, I.; Khodakov, A. Y.; Durand, D.; Zholobenko, V. L. New Insights into the Initial Steps of the Formation of SBA-15 Materials: An in Situ Small Angle Neutron Scattering Investigation. *Chem. Commun.* **2007**, *0*, 834–836.
- (40) Manet, S.; Schmitt, J.; Impérator-Clerc, M.; Zholobenko, V.; Durand, D.; Oliveira, C. L. P.; Pedersen, J. S.; Gervais, C.; Baccile, N.; Babonneau, F.; Grillo, I.; Meneau, F.; Rochas, C. Kinetics of the Formation of 2D-Hexagonal Silica Nanostructured Materials by Nonionic Block Copolymer Templating in Solution. *J. Phys. Chem. B* **2011**, *115*, 11330–11344.
- (41) Sun, J.; Ding, M.; Zhang, H.; Wang, C.; Bao, X.; Su, D. S.; Klein-Hoffman, A.; Weinberg, G.; Mann, S. Phase Evolution in the Alkene-P123-Water-TEOS Quadro-Component System: A Feasible Route to Different Complex Mesostructured Materials. *J. Mater. Chem.* **2006**, *16*, 1507–1510.

- (42) Nagarajan, R. Solubilization of "Guest" Molecules into Polymeric Aggregates. *Polym. Adv. Technol.* **2001**, *12*, 23–43.
- (43) Nagarajan, R. Solubilization of Hydrocarbons and Resulting Aggregate Shape Transitions in Aqueous Solutions of Pluronic (PEO-PPO-PEO) Block Copolymers. *Colloids Surf., B* **1999**, *16*, 55–72.
- (44) Iler, R. K. In *The Chemistry of Silica*; Wiley: New York, 1979.
- (45) Brinker, C. J. Hydrolysis and Condensation of Silicates: Effects on Structure. *J. Non-Cryst. Solids* **1988**, *100*, 31–50.
- (46) Nadargi, D. Y.; Kalesh, R. R.; Rao, A. V. Rapid Reduction in Gelation Time and Impregnation of Hydrophobic Property in the Tetraethoxysilane (TEOS) Based Silica Aerogels Using NH<sub>4</sub>F Catalyzed Single Step Sol–Gel Process. *J. Alloys Compd.* **2009**, *480*, 689–695.
- (47) Boissière, C.; Martines, M. A. U.; Tokumoto, M.; Larbot, A.; Prouzet, E. Mechanisms of Pore Size Control in MSU-X Mesoporous Silica. *Chem. Mater.* **2003**, *15*, 509–515.
- (48) Kabalnov, A.; Olsson, U.; Wennerstroem, H. Salt Effects on Nonionic Microemulsions Are Driven by Adsorption/Depletion at the Surfactant Monolayer. *J. Phys. Chem.* **1995**, *99*, 6220–6230.
- (49) Linton, P.; Rennie, A. R.; Alfredsson, V. Evolution of Structure and Composition during the Synthesis of Mesoporous Silica SBA-15 Studied by Small-Angle Neutron Scattering. *Solid State Sci.* **2011**, *13*, 793–799.
- (50) Van Der Voort, P.; Ravikovitch, P. I.; De Jong, K. P.; Benjelloun, M.; Van Bavel, E.; Janssen, A. H.; Neimark, A. V.; Weckhuysen, B. M.; Vansant, E. F. A New Templated Ordered Structure with Combined Micro- and Mesopores and Internal Silica Nanocapsules. *J. Phys. Chem. B* **2002**, *106*, 5873–5877.
- (51) Khodakov, A. Y.; Zholobenko, V. L.; Impérator-Clerc, M.; Durand, D. Characterization of the Initial Stages of SBA-15 Synthesis by in Situ Time-Resolved Small-Angle X-Ray Scattering. *J. Phys. Chem. B* **2005**, *109*, 22780–22790.
- (52) Bernards, T. N. M.; van Bommel, M. J.; Boonstra, A. H. Hydrolysis-Condensation Processes of the Tetra-Alkoxy silanes TPOS, TEOS, and TMOS in some Alcoholic Solvents. *J. Non-Cryst. Solids* **1991**, *134*, 1–13.
- (53) Linton, P.; Hernandez-Garrido, J.; Midgley, P. A.; Wennerström, H.; Alfredsson, V. Morphology of SBA-15-Directed by Association Processes and Surface Energies. *Phys. Chem. Chem. Phys.* **2009**, *11*, 10973.
- (54) Linton, P.; Wennerstrom, H.; Alfredsson, V. Controlling Particle Morphology and Size in the Synthesis of Mesoporous SBA-15 Materials. *Phys. Chem. Chem. Phys.* **2010**, *12*, 3852–3858.
- (55) Wanka, G.; Hoffmann, H.; Ulbricht, W. Phase Diagrams and Aggregation Behavior of Poly(Oxyethylene)-Poly(Oxypropylene)-Poly(Oxyethylene) Triblock Copolymers in Aqueous Solutions. *Macromolecules* **1994**, *27*, 4145–4159.
- (56) Alexandridis, P.; Holzwarth, J. F. Differential Scanning Calorimetry Investigation of the Effect of Salts on Aqueous Solution Properties of an Amphiphilic Block Copolymer (Poloxamer). *Langmuir* **1997**, *13*, 6074–6082.
- (57) Sun, J.; Ma, D.; Zhang, H.; Jiang, F.; Cui, Y.; Guo, R.; Bao, X. Organic Molecule-Modulated Phase Evolution of Inorganic Mesostuctures. *Langmuir* **2008**, *24*, 2372–2380.
- (58) Diat, O.; Roux, D.; Nallet, F. "Layering" Effect in a Sheared Lyotropic Lamellar Phase. *Phys. Rev. E* **1995**, *51*, 3296–3299.
- (59) Lettow, J. S.; Lancaster, T. M.; Glinka, C. J.; Ying, J. Y. Small-Angle Neutron Scattering and Theoretical Investigation of Poly(Ethylene Oxide)-Poly(Propylene Oxide)-Poly(Ethylene Oxide) Stabilized Oil-in-Water Microemulsions. *Langmuir* **2005**, *21*, 5738–5746.
- (60) Manet, S.; Lecchi, A.; Impérator-Clerc, M.; Zholobenko, V.; Durand, D.; Oliveira, C. L. P.; Pedersen, J. S.; Grillo, I.; Meneau, F.; Rochas, C. Structure of Micelles of a Nonionic Block Copolymer Determined by SANS and SAXS. *J. Phys. Chem. B* **2011**, *115*, 11318–11329.